SPE-194353-MS

Case Study of a Landing Location Optimization within a Depleted Stacked Reservoir in the Midland Basin

Cyrille Defeu, Ryan Williams, and Dan Shan, Schlumberger; Joel Martin, Dave Cannon, Kyle Clifton, and Chad Lollar, Diamondback Energy

This paper was prepared for presentation at the SPE Hydraulic Fracturing Technology Conference and Exhibition held in The Woodlands, Texas, USA, 5-7 February 2019.

Abstract

Unconventional plays across the US are often made of stacked pays, typically ranging from a few hundred to thousands of feet thick. These stacked pay intervals are generally segregated into different formations as dictated by differences in geology, mineralogy, rock fabric, and fluid type. This proves to be a challenge because many stacked/staggered horizontal wells are required to provide effective coverage of the reservoir. Selecting the right landing location can become even more challenging in an environment with existing producing wells in adjacent formations because pressure depletion and its associated effects on fracture propagation necessitate consideration of vertical spacing and time.

In this study, we outline an integrated approach that addresses a four-dimensional horizontal well placement challenge in the Midland basin's Wolfcamp A formation using advanced hydraulic fracture modeling to calibrate hydraulic fracture geometries and history match five producing wells in both Lower Spraberry and Wolfcamp B.

The optimal landing location within the Wolfcamp A was determined based on an assessment of reservoir quality, rock mechanics, unique structural features, and depletion effects. These data were then combined to form a 4D geomodel that enabled a completion optimization study via modeling of the resulting complex hydraulic fracture geometry and subsequent hydrocarbon production.

This integrated workflow, using a wide array of high-quality datasets and the input of experts from multiple disciplines, yielded a comprehensive assessment and clear recommendations for this challenging partially depleted stacked pay interval. Although this study is specific to the Midland basin's Lower Spraberry and Wolfcamp A and B formations, many sections of the workflow apply to other basins and their unique strata.

Introduction

The Midland basin of West Texas, USA, hosts the prolific stacked Spraberry and Wolfcamp formations. Production from these formations has been growing for years, despite the concurrent challenges in crude oil pricing and/or production constraints. As operators of these formations have transitioned from "lease holding" well placement (i.e., parent wells) to infill well placement (i.e., child wells), production challenges for both the parent and child wells have been regularly experienced. This phenomenon is not unique to the Midland basin and has been observed in all major unconventional formations across the US.

As described in Lindsay et al. (2018), child wells in the Wolfcamp outproduce their parent wells in 34% of the cases and only 21% of the cases when normalized by pounds of proppant pumped per foot of lateral. However, this effect drops in severity as the well spacing distance increases. This is because of the underlying cause of the production underperformance of child wells—pressure depletion.

As pressure depletes within the reservoir due to production of the parent wells, there is a localized change in geomechanical stresses. If not properly accounted for during the design of a child completion, these (lower) stresses can result in unanticipated changes to the fracture dimensions during hydraulic stimulation of the reservoir. In extreme cases, this can result in fracture reorientation (Marongiu-Porcu et al. 2015), but it typically results in fracture asymmetry for the child well. This asymmetry is normally characterized as a fracture system that preferentially grows towards the pre-existing parent well, with some level of observed pressure communication. Unintended communication can often irreversibly damage the parent well's production and simultaneously lead to poor child well production due to the newly created fracture geometry being hosted in depleted rock.

This effect can be predicted by pressure matching parent well completions to determine their stimulated rock volume and then production history matching the wells to simulate formation pressure depletion. In cases where vertical containment is poor, the same workflow must be followed for over/underlying wells. A recalculation of the in-situ stress state during production can be generated, which can then be used to simulate a child well completion. This workflow was implemented to determine proper placement and stimulation of a Wolfcamp A well following the stimulation and production of three overlying Lower Spraberry wells and two underlying Wolfcamp B wells (Fig. 1).

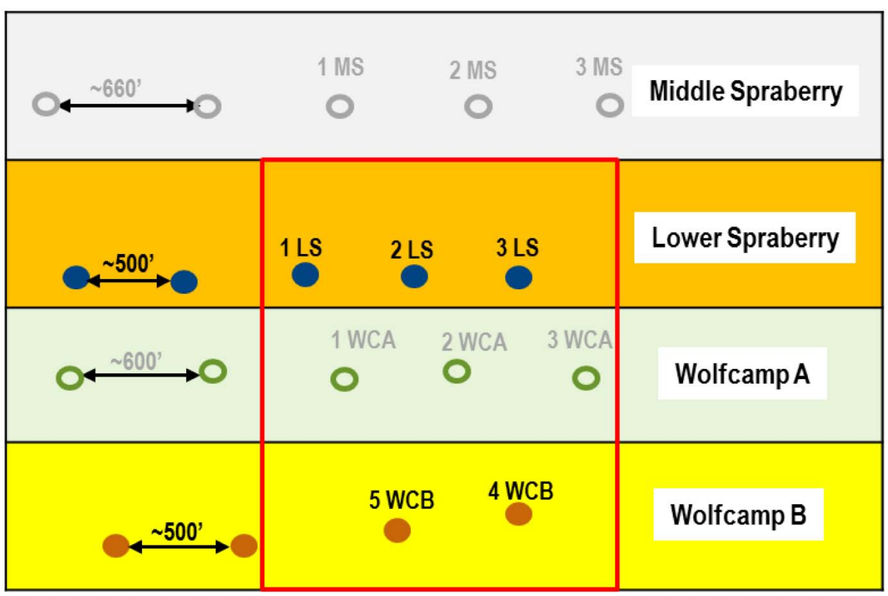

Figure 1—Gun barrel view of wells contained within the Middle Spraberry (gray), Lower Spraberry (blue), Wolfcamp A (green), and Wolfcamp B (orange). Solid dots indicate wells that have been drilled and completed whereas hollow dots indicate planned landing locations. Area in red indicates the zone of interest for the study.

As shown in Fig. 1, the section being studied shows the vertical and horizontal layout of wells that have been completed (solid colored circles) and wells to be drilled and completed (hollow colored circles). Wells in blue in the red box represent the Lower Spraberry completions that were matched as part of the workflow outlined in this paper, whereas wells in orange represent the wells landed and completed in the Wolfcamp B. Finally, wells in green and gray represent wells planned for drilling and completion in the

Wolfcamp A and Middle Spraberry, although Middle Spraberry completions were not considered in this project. Average lateral well spacing was approximately 600 ft, with vertical spacing between the Lower Spraberry and Wolfcamp B wells being 500 ft.

All five wells that were previously completed and studied as a part of this work were pumped with slickwater at 95 bbl/min through four clusters per stage. All Lower Spraberry wells had 40-ft cluster spacing, 2,800 gal of fluid pumped per foot of lateral, and 1,900 lbm of proppant pumped per foot of lateral. The Wolfcamp B wells had varying cluster spacing, with one being 40 ft and the other being 60 ft. The quantity of fluid and proppant pumped per foot of lateral for the Wolfcamp B wells was lower than the Spraberry wells, at 1,800 gal and 1,200 lbm, respectively.

The five wells were drilled and completed at different times, starting with the Wolfcamp B wells, 6 months apart, in summer/winter of 2014. Well 4WCB was initially produced with an electric submersible pump then a rod pump, whereas 5WCB was produced with gas lift. The Lower Spraberry wells were all completed simultaneously in winter 2015, with electric submersible pumps being installed in each for production.

Methodology

This study is based on the multiwell advanced workflow discussed by Gakhar et al. (2016), Malpani et al. (2015), and Ejofodomi et al. (2015) and adapted to infill well situations by Defeu et al. (2018) as shown in Fig. 2. The workflow is based on eight steps divided into two main processes: the parent process during which the model is calibrated, and the child process during which infill is introduced to the calibrated model and optimized accordingly.

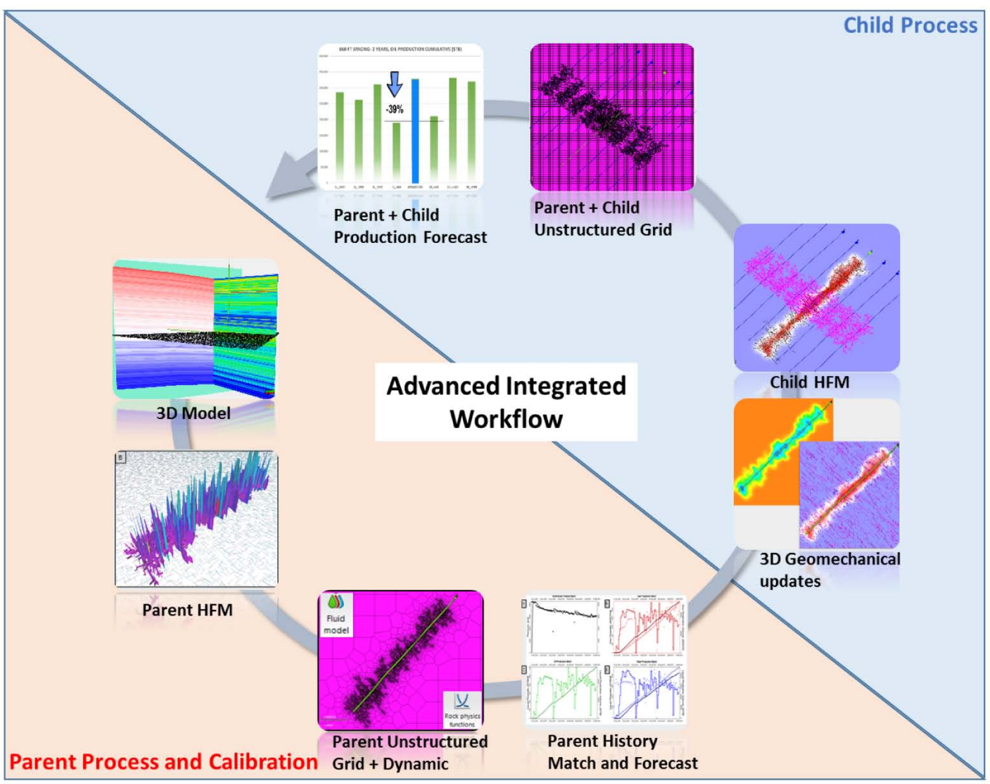

Figure 2—Advanced integrated workflow showing parent process and child process.

Development of a Regional Model

The framework for this integrated study is a 3D geomechanical model of the area of interest that consists of a total of five parent wells, of which three are in the Lower Spraberry and two are in Wolfcamp B. This model is built by bringing together logs (Fig. 3) and seismic surfaces to account for deformation within the study area.

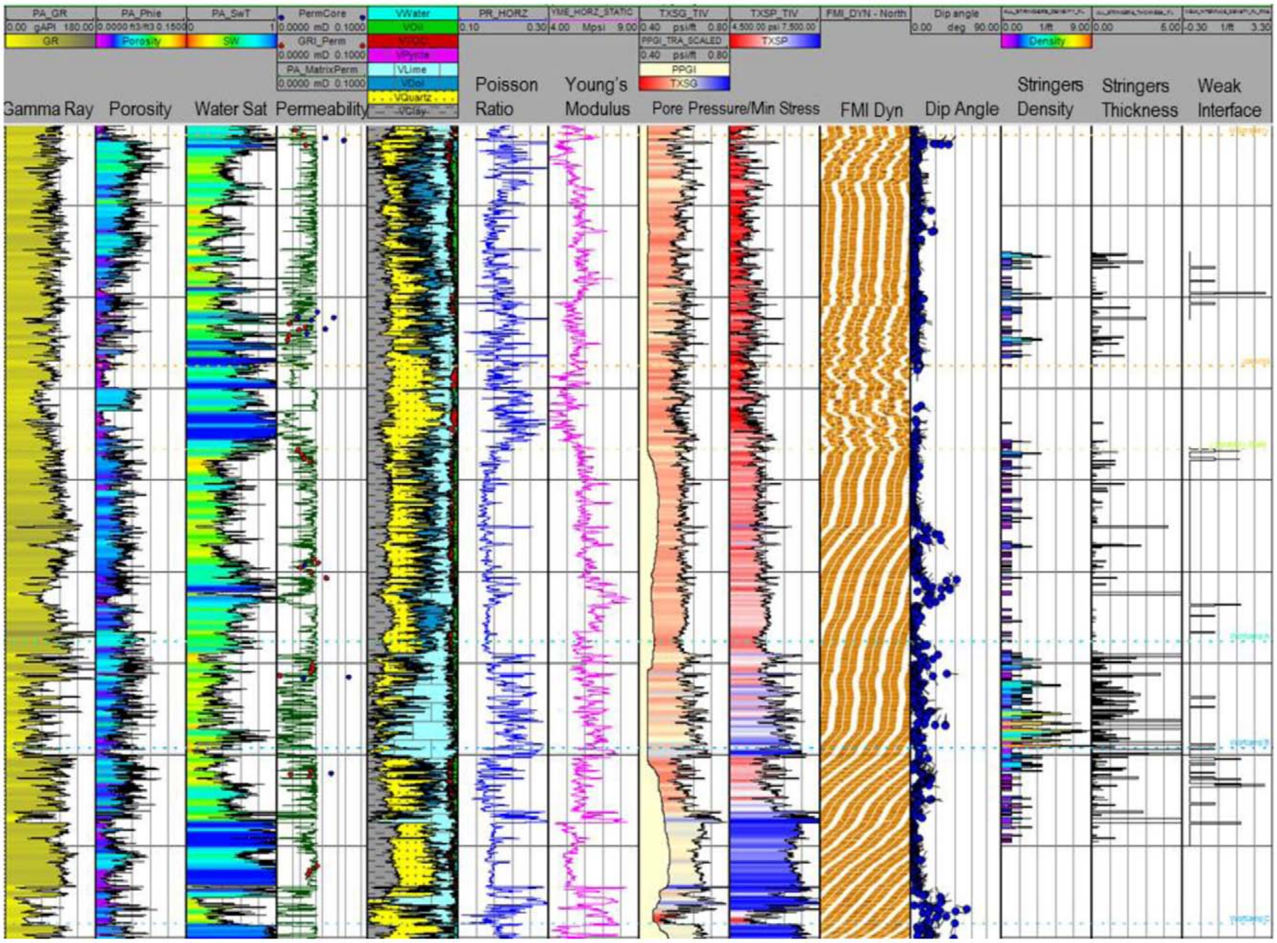

Figure 3—3D model input data.

For mechanical properties, measurements from an acoustic scanning platform were used to calculate bulk moduli, with pore pressure being calibrated with available diagnostic fracture injection test (DFIT) analysis. Subsequent parameters such as Biot's constant, Young's modulus, Poisson's ratio, and minimum stress were calculated, and maximum stress magnitude and angle were estimated based on drilling-induced fractures from image logs. Water saturation, porosity, and permeability were calculated based on petrophysical logs and elemental analysis of the reservoir and then calibrated with available core data.

Structural features of the area of interest were used to generate surfaces (Fig. 4) derived from depth conversion of the seismic measurements tied to well tops in the area. Other structural features such as natural fractures and rock fabric will be discussed in the next section.

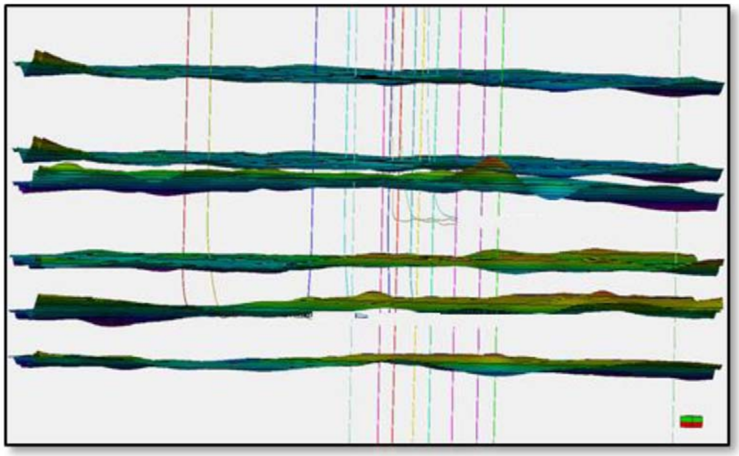

Figure 4—Structural surfaces running from Middle Spraberry to Wolfcamp C.

Fig. 5 shows the resulting 3D grid with high resolution in the vertical direction to capture subtle property changes within the layers. Properties shown include minimum stress, total water saturation, and gamma ray. The 3D mechanical earth model is used directly as an input into a hydraulic fracture simulator that is capable of modeling the complex interaction between the propagating fractures and the existing natural fissure network. Additionally, the model is populated with the actual completion parameters for fluid/proppant volumes, rates, and stage/perforation geometries for each well (Wallace et al. 2016).

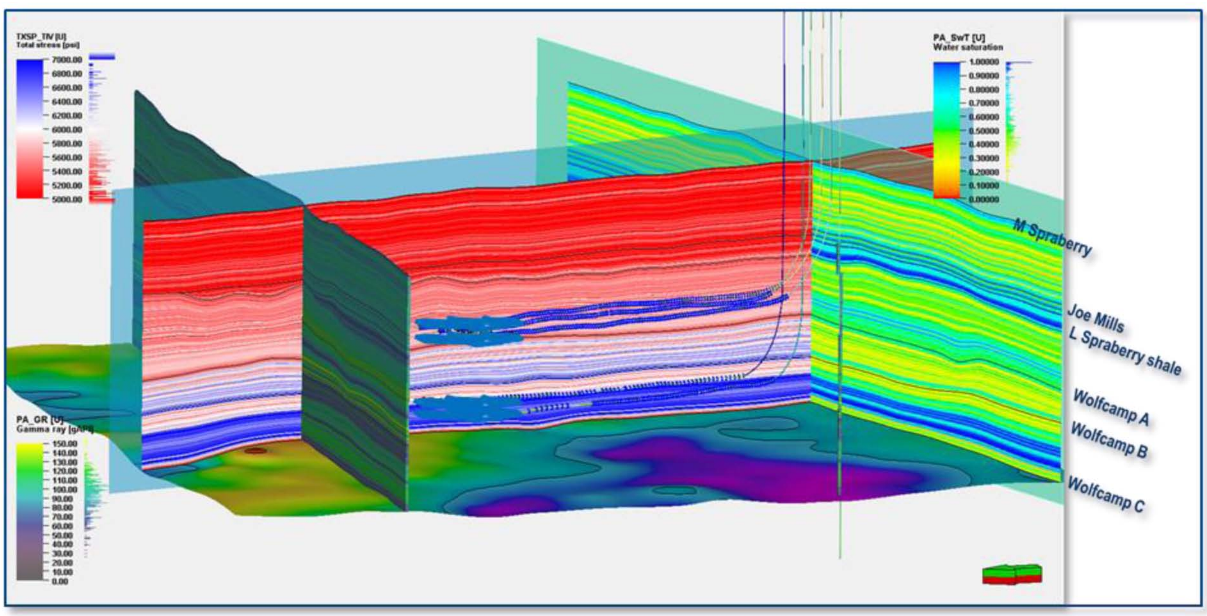

Figure 5—3D model of the area of interest with the five parent wells.

Microseismic data were acquired during the completions of a Lower Spraberry well and a Wolfcamp B well near to the study area. Fig. 6 shows the results acquired during the stimulation of the Lower Spraberry well. The data indicated good containment within the Lower Spraberry, with very few events occurring in the Wolfcamp A. Likewise, microseismic data from the Wolfcamp B well indicated good containment, with very few events occurring in the Wolfcamp A. See Diaz et al. (2018) for a more thorough discussion.

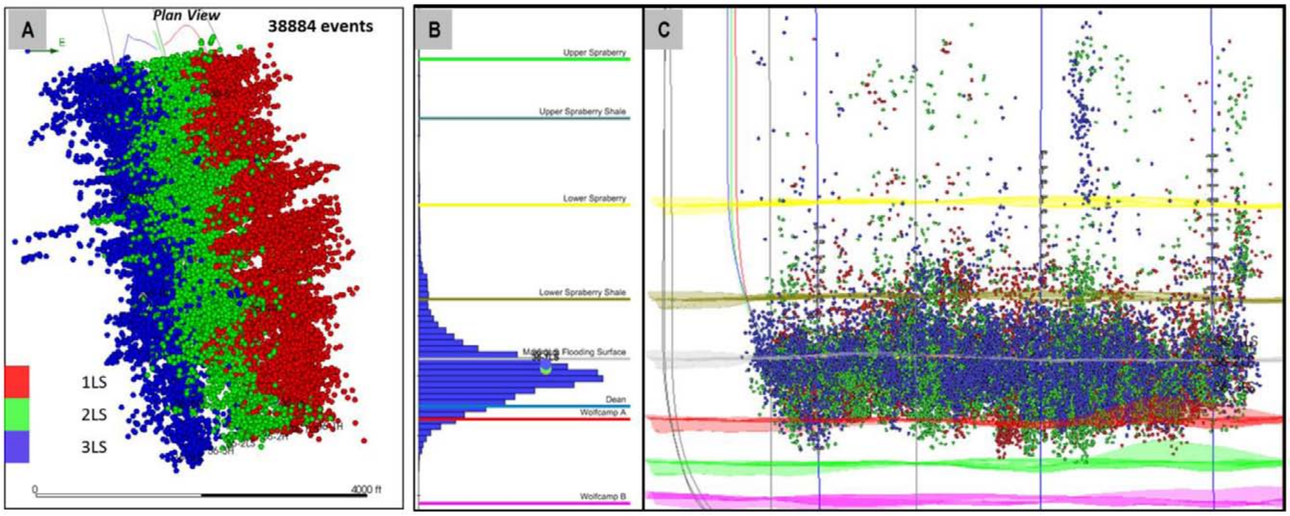

Figure 6—Lower Spraberry offset wells microseismic data. (A) Top view of events of offset wells. (B) Histogram of in the vertical direction showing most events within Lower Spraberry shale. (C) Sideview of microseismic events.

Hydraulic Fracture Calibration

Due to the large scope of the project and associated complexity of the computations, a 960-ft subset of the pumped stages in each lateral was selected. The stages selected in each well resided within the same volumetric section of the Spraberry/Wolfcamp stack to result in a volume containing fractures from all five wells. This volume contained three Lower Spraberry wells, each consisting of six stages and 24 perforation clusters, and two Wolfcamp B wells, each consisting of four stages and 16 clusters. Treating pressures and instantaneous shut-in pressures (ISIPs) were remarkably similar within the lateral section of each well (as shown in Fig. 7 for well 1LS stage 18 to 22), indicating homogeneity in fracture geometries. These stimulating pressure observations were backed up with microseismic data from other wells in the area, indicating homogeneity in the fracture geometries within each well.

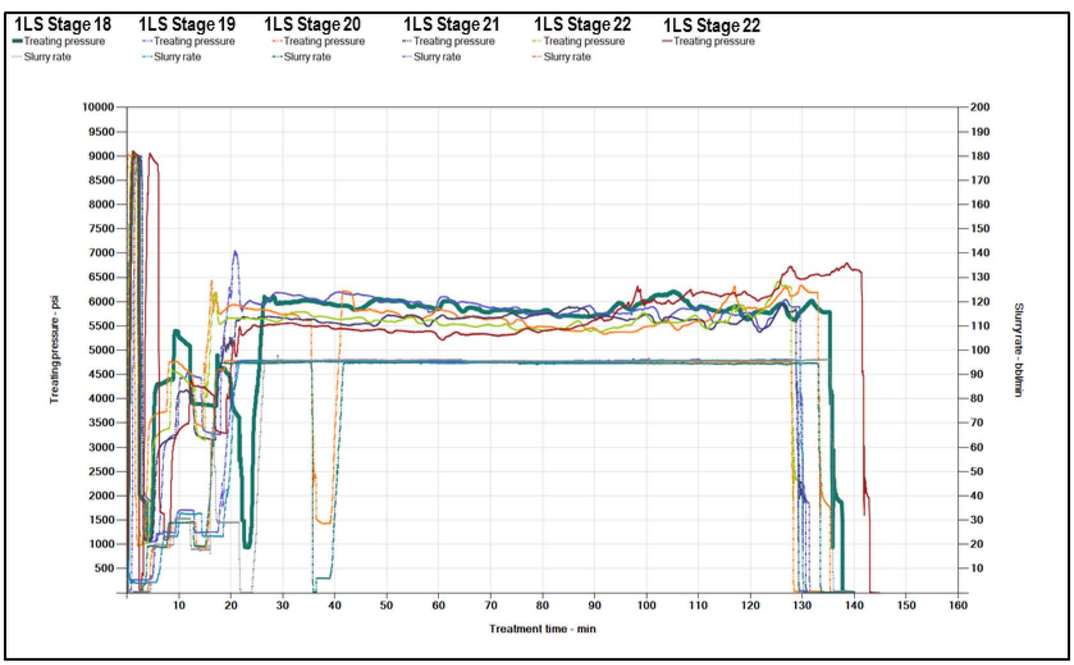

Figure 7—Example of treating plots for selected stages of a Lower Spraberry well 1LS

Microseismic data also indicated fracture complexity, rather than planar fracture geometries. Use of formation microimager data (Fig. 8A) enabled the identification and characterization of natural fractures within the zone of interest, and this information was used to develop a discrete fracture network (DFN) as shown in Fig. 8B for incorporation into fracture models. Two groups of natural fractures were identified within the pilot well, oriented at 90° and 40°. A 10% standard deviation was assumed for these orientations, which was reflected in the observations by the logging tool. The density of the natural fractures within the pilot well was 3:1, with fractures oriented at 90° being three times more frequently observed than those oriented at 40°. The density was initially set up as being one feature every 100 ft for the 90° fractures, and one feature every 300 ft for the 40° fractures. These fracture densities, as well as the fracture lengths of 120 ft used in the model, have been historically used and well matched in the area before.

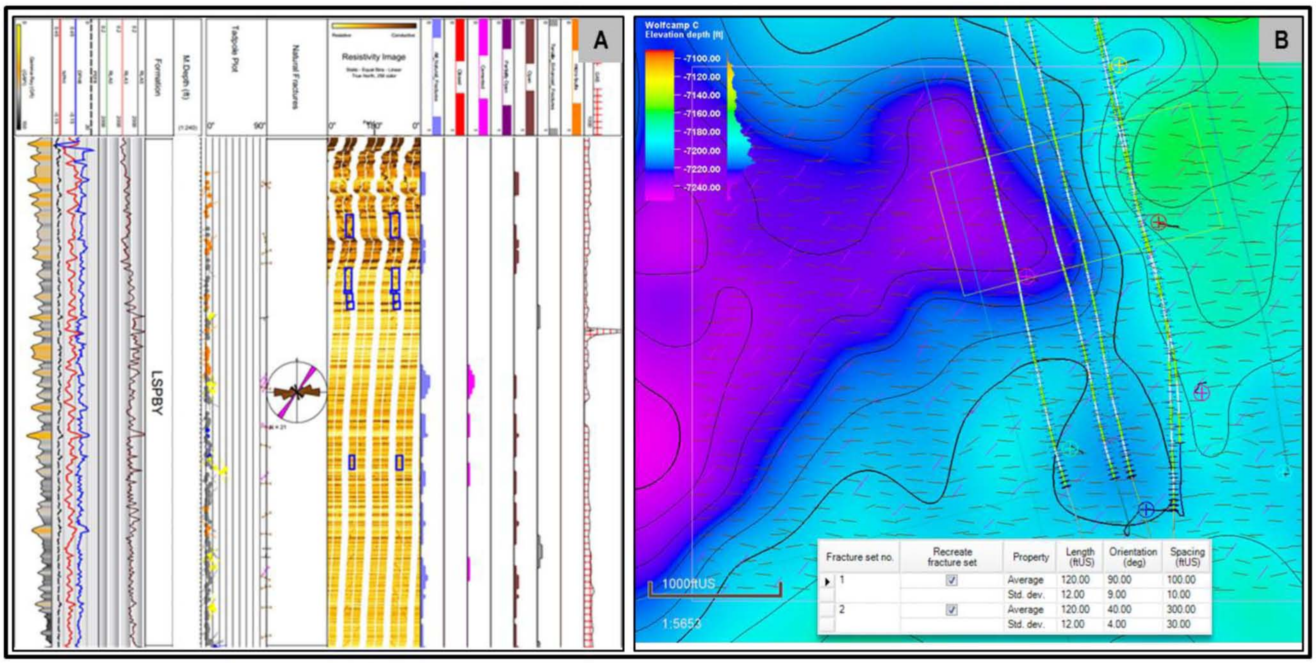

Figure 8—Developing the distributed fracture network (DFN) from the formation microimager log. (A) Image log identifying two sets of natural fractures (cemented and open) in the Lower Spraberry. (B) DFN created using parameters from the image log.

Model Mismatch and Identification of Barriers from the Image Log

Although the microseismic data backed up the homogeneity in fracture pressures, it indicated a discrepancy in fracture propagation between field observations and initial simulations. Predictions of height growth for the Lower Spraberry and Wolfcamp B wells were inconsistent with field observations, often by more than 100 ft. Microseismic inversion suggested the presence of previously unrecognized features that were controlling fracture containment, leading to further study of the logs. Analysis of the formation image data used for determining natural fracture presence and orientation was also used to identify any features that could act as fracture barriers that were incapable of being detected using traditional sonic tools and therefore not incorporated into initial mechanical earth models (MEMs). As described by Diaz et al. (2018), resistivity images were used to identify weak interfaces, weak beds, and stringers that could potentially restrict the vertical growth of a hydraulic fracture. This was done by evaluating drilling-induced fractures (DIFs) and how they interacted with features within the rock column.

The rock fabric analysis showed that the thickest stringers (tight beds), already captured by the MEM, had the largest effect on DIF behavior. As a result, focus was given to weak interfaces to see if their presence was sufficient to explain the field observations. The flags related to weak beds/weak interfaces were converted into a lamination density log and integrated into the existing hydraulic fracturing workflow as an additional tuning parameter. This tuning parameter applies a measure of horizontal offset when a fracture intersects a given lamination (X. Weng, pers. commun., 2012), enabling data-driven matching of both microseismic and fluid pressure measurements.

Use of this offset parameter resulted in a dramatic change in fracture height and length while honoring the net pressure prediction. Using the rock fabric analysis workflow, swarms of weak beds/weak interfaces were identified in the Lower Spraberry and the bottom of the Wolfcamp A and likely explain why containment could not be achieved using acoustic logs alone. All stages in the five wells in the Lower Spraberry and Wolfcamp B were matched using the same tuning parameter for weak beds/interfaces (i.e., it was not varied on a stage-by-stage basis). This parameter enabled matching of each stage with minor adjustment to fluid and proppant friction values, giving confidence that the model was representative of the stimulated rock volume. Fig. 9 shows the treating pressure match obtained for stage 18 of Lower Spraberry well 1LS, the orange line is surface treating pressure as measured and the green line is the simulated treating pressure.

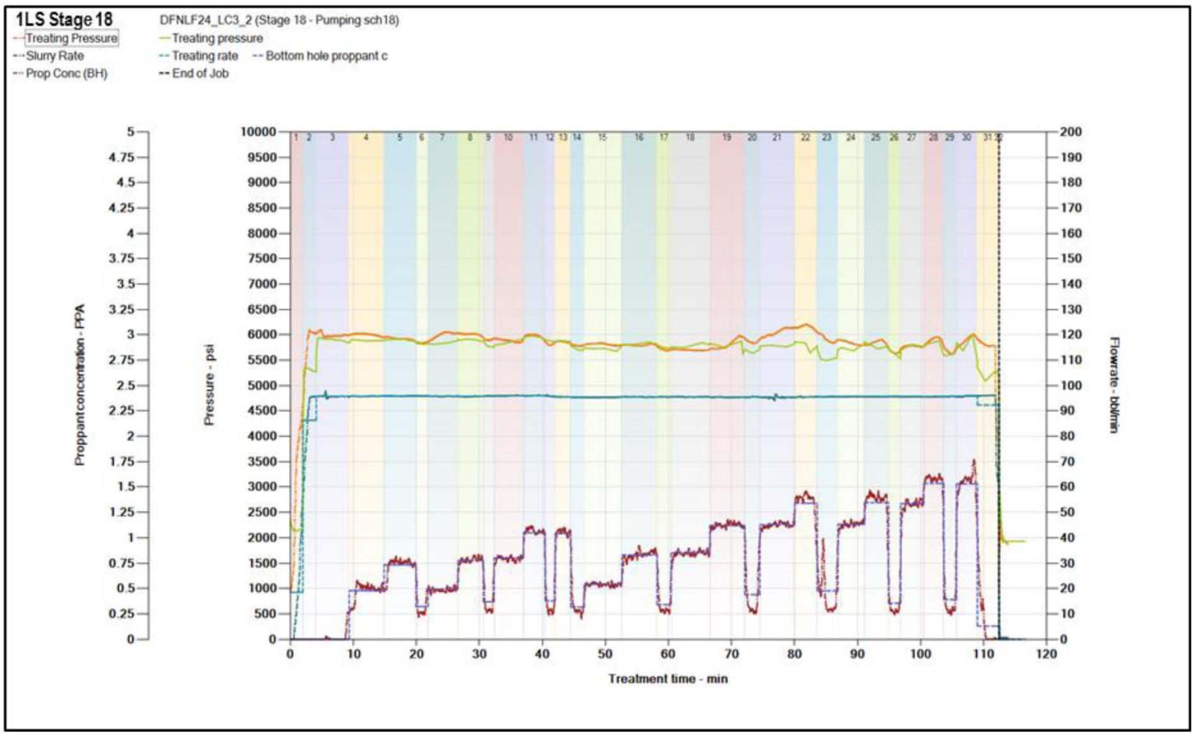

Figure 9—Example of treating pressure match for 1LS stage 18.

Production Modeling and Matching

The resulting complex hydraulic fracture geometry network for both the Lower Spraberry and Wolfcamp B wells was converted into an unstructured grid using an autogridding algorithm that accurately captures the hydraulic fracture footprint as well as proppant distribution within the fractures. A total of 5 million cells were generated for the five wells in the study. This new static grid containing petrophysics and pressure data is combined with compaction tables, relative permeability, and PVT data to create a dynamic model that is used to history match the five wells in the study. Results of the history match are shown on Fig. 10 (rates and pressure) and Fig. 11 (cumulative).

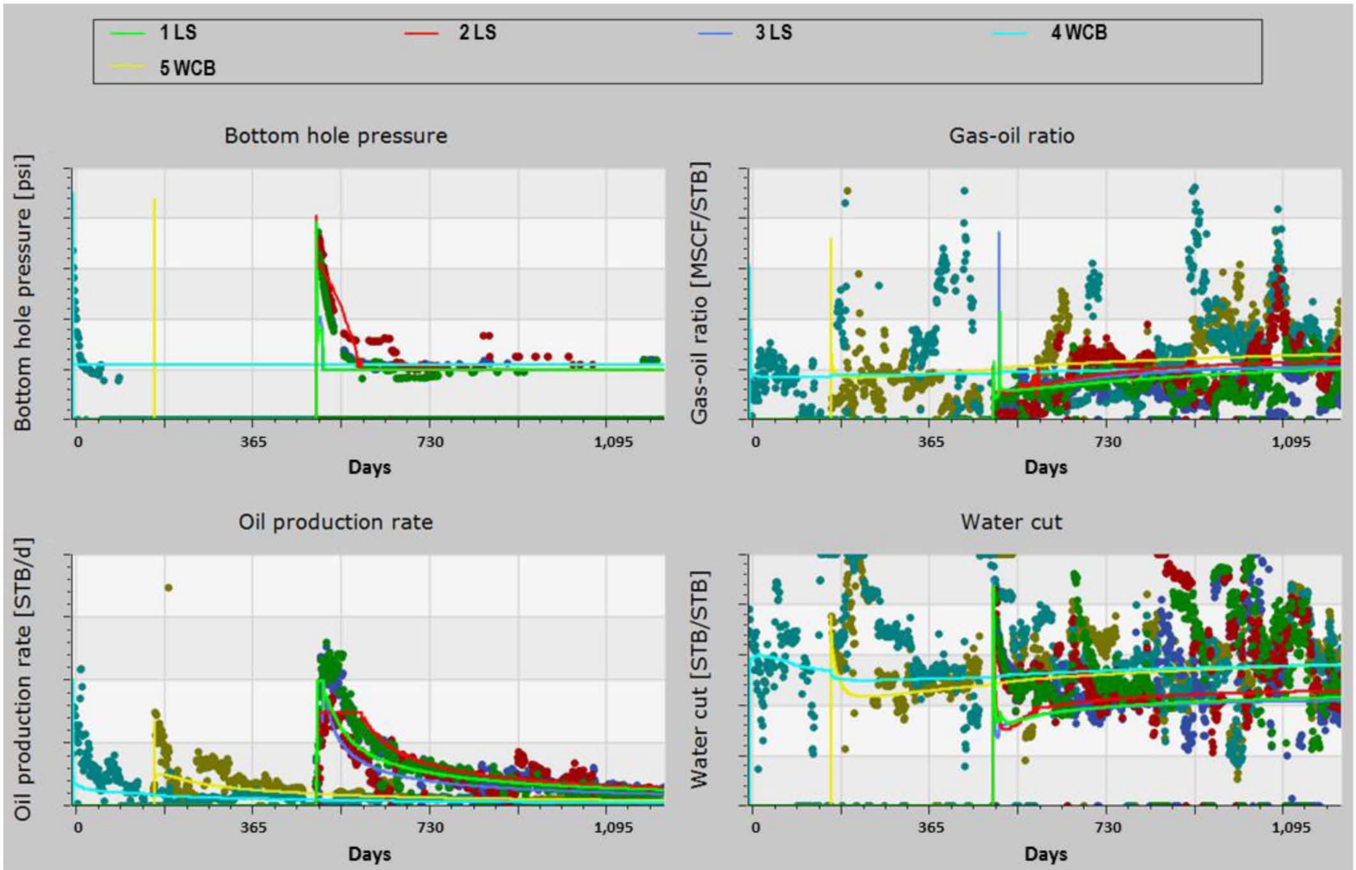

Figure 10—Production history match plots for the five wells showing bottomhole pressure, oil rate, gas-oil ratio (GOR), and water cut.

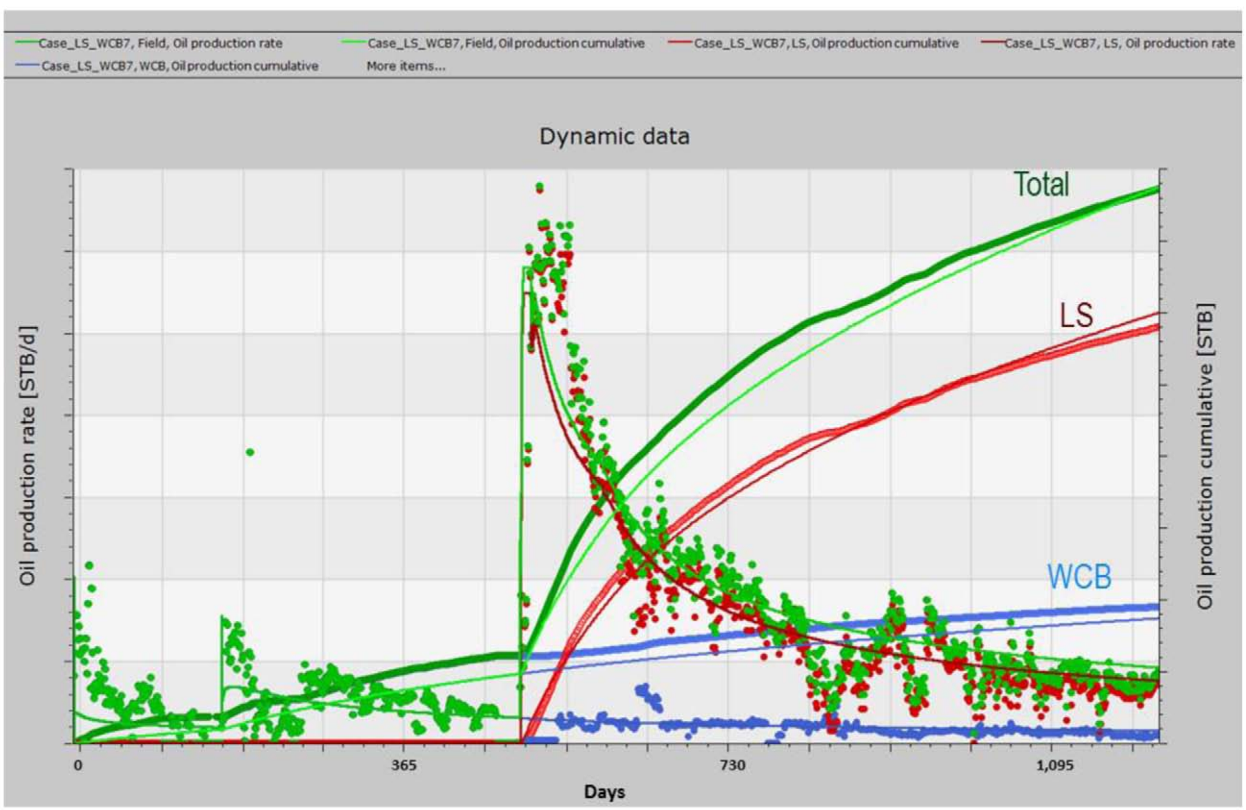

Figure 11—Oil production rate and cumulative oil volume for five wells.

To achieve the match, calculated bottomhole pressures are used when surface tubing or pump intake pressure is available. When bottomhole pressure data are not available, a constant bottomhole pressure is assumed to produce the wells, with the volume being matched by adjusting parameters such as matrix permeability, fracture contribution, and critical saturation parameters.

Depletion of Wolfcamp A

The resulting depletion profile from Lower Spraberry and Wolfcamp B wells is illustrated in Fig. 12 where grid cells are filtered with respect to the change in pressure from initial condition. In this case, a pressure change of 10% or higher is captured after the system has been produced for 3 years. It is clear from this 3D illustration that although no well was landed in Wolfcamp A, it has been depleted to some degree by wells landed in adjacent formations.

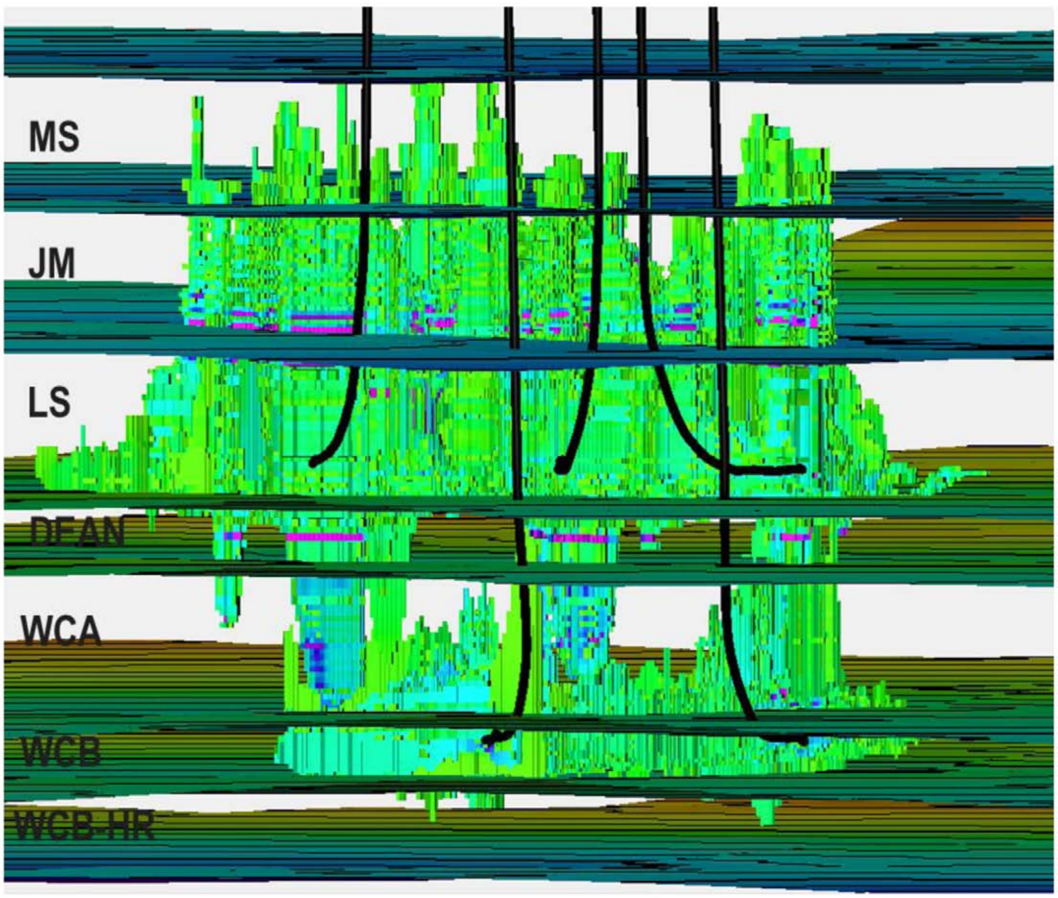

Figure 12—3D view of the pressure depletion profile after producing three Lower Spraberry wells and two Wolfcamp B wells.

Fig. 13 shows the production contribution from each set of wells from the adjacent formations to Wolfcamp A. Wolfcamp A contributes up to 7% of oil, 6% of gas, and 2% of water to Lower Spraberry wells, whereas for Wolfcamp B wells, the contribution is 23% of oil, 22% of gas, and 3% of water. This partial depletion of Wolfcamp A and adjacent formations needs to be accounted for when planning new wells targeting the Wolfcamp A.

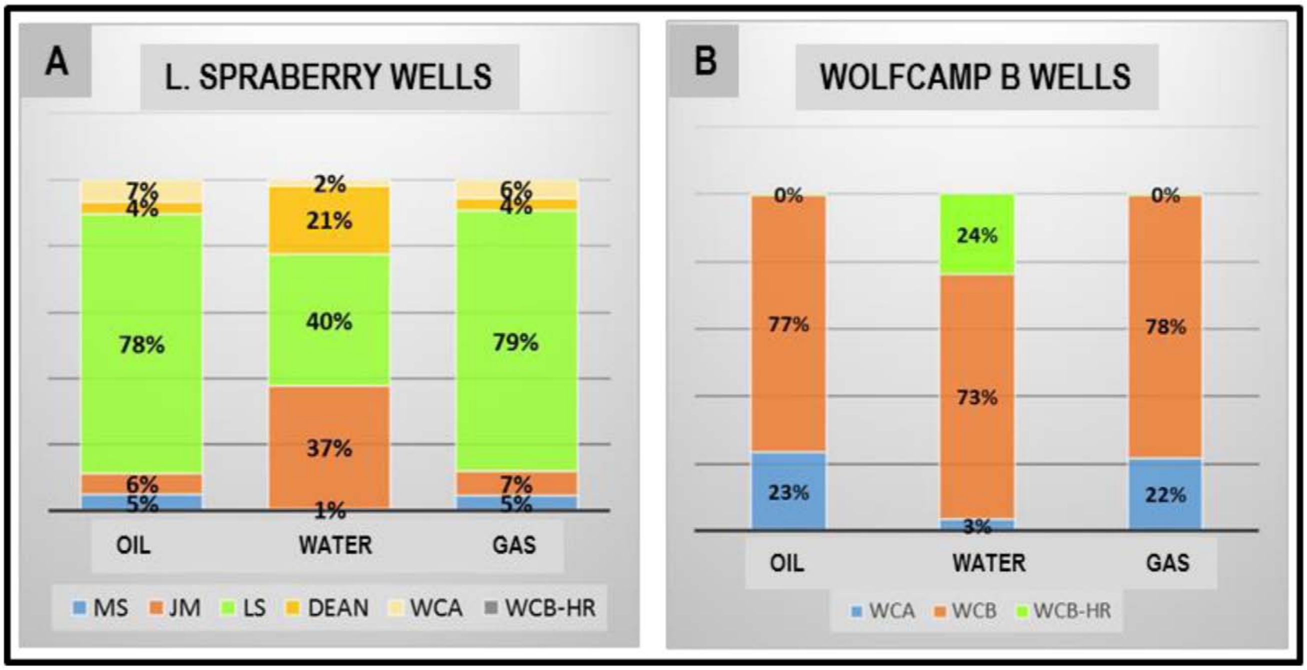

Figure 13—Production contribution from different benches. (A) Three Lower Spraberry wells. (B) Two Wolfcamp B wells.

Updating Local Stresses due to Depletion

Fluid pressure partially supports the stress acting on the reservoir element. If the fluid pressure drops, as fluid is removed from the reservoir as a result of production, the support is reduced, and the reservoir elements want to contract. Because reservoir elements cannot contract laterally, pore pressure depletion causes stress magnitude change and azimuthal realignment [Martinez et al. (2012) cited by Ajisafe et. al. (2017) and Defeu et. al. (2018)]. This alteration of the geomechanical properties with reservoir pressure depletion due to production overtime is captured using the finite element method (FEM) to solve for magnitude and orientation of the stresses. As such, the geomechanical simulations carried out in this study assume elastic deformation behavior as a first-order approximation. The simulator then computes the corresponding 3D change in stress, deformation, and rock displacement in the reservoir and beyond in the adjacent rock formation. In this way, the spatial and temporal changes in the in-situ stress field from parent wells production are computed (Defeu et al. 2018). The geomechanical simulator outputs a 3D model updated with in-situ stress magnitude and orientation corresponding to reservoir pressure after production from the parent wells (Gakhar et al. 2017). The updated 3D MEM is used as the starting point to simulate parent and child wells in interaction (Defeu et al. 2018).

Fig. 14 and Fig. 15 show the associated stress change corresponding to the pressure depletion illustrated in Fig. 12. Most of the stress change occurs in close proximity to the producing wellbores. This does not result in a change in the stress orientation because the stress anisotropy was high. The majority of the stress change occurs within the Lower Spraberry and Wolfcamp B formations, with less predicted within the Wolfcamp A. However, the majority of the Wolfcamp A remains at or near virgin conditions due to the lack of pressure depletion within the zone.

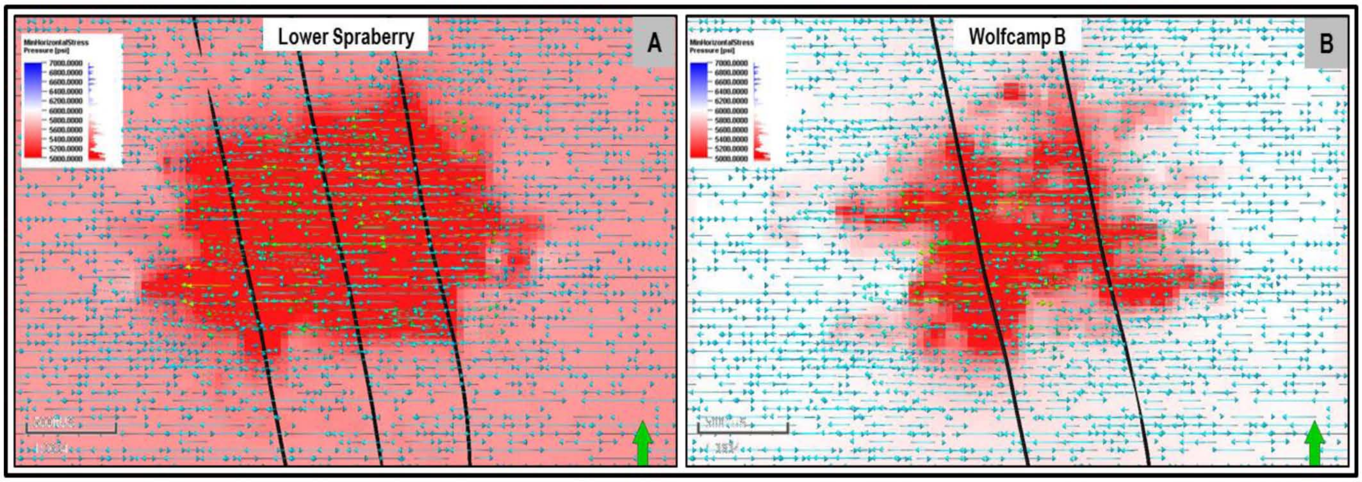

Figure 14—Top view at the well layers of updated minimum stress magnitude and maximum stress direction (horizontal arrows). (A) Lower Spraberry. (B) Wolfcamp B.

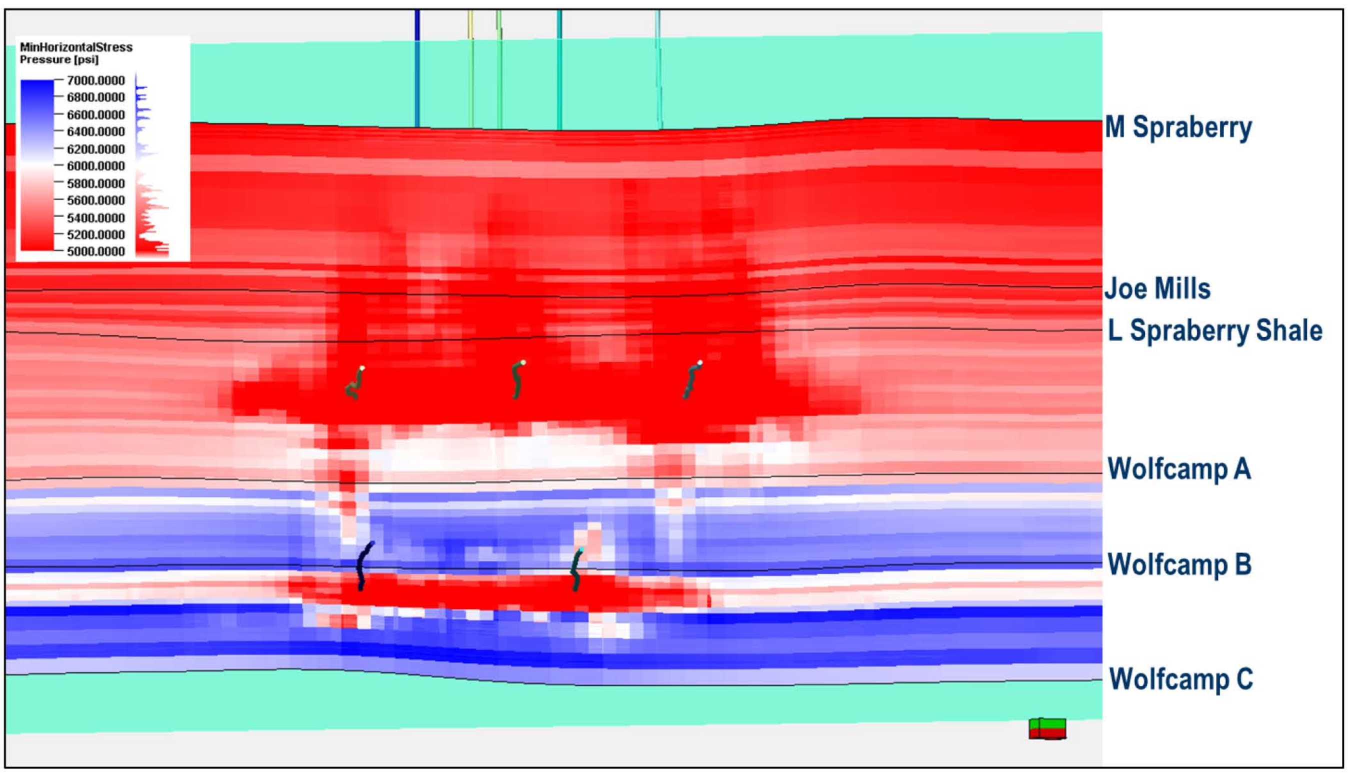

Figure 15—Gun barrel view of wells showing updated minimum stress.

Lateral Landing Point Evaluation

After the production history match of every well has been obtained and integrated into the calculation of updated in situ stress, its effect on fracture propagation from new wells landed in the Wolfcamp A can be assessed (Fig. 16). Three different landing points were evaluated, with the depths being 260 ft (target 1), 335 ft (target 2), and 405 ft below (target 3) the landing point of the previously completed Lower Spraberry wells. Fracture propagation from these laterals were simulated using a base completion design used on other wells in the area: a 100% slickwater design containing 320,000 lbm of 100-mesh and 40/70 proppant.

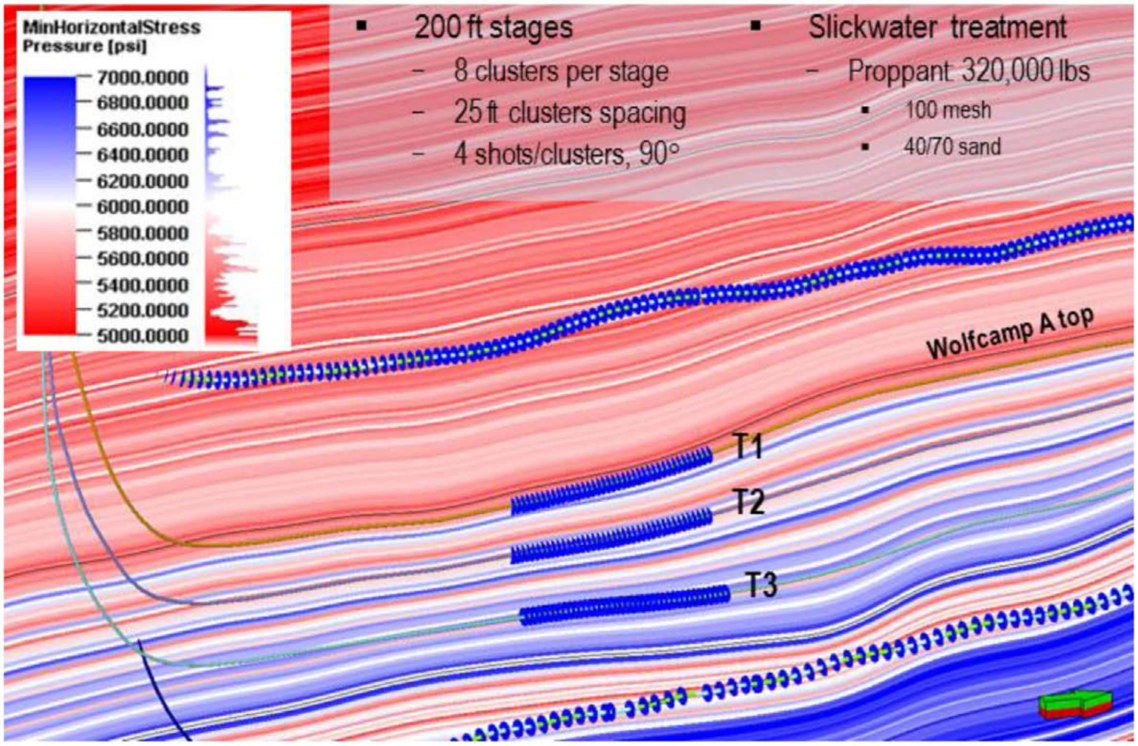

Figure 16—Wolfcamp A landing targets and base completion summary.

Simulations of these three scenarios showed that shallow landing points resulted in fracture height growth into the Lower Spraberry, and potentially detrimental fracture hits to parent wells (Fig. 17). This also resulted in reduced fracture lengths and poorer production performance from the Wolfcamp A. Fractures initiated from deeper landing locations, specifically from the higher stressed rock of the lower Wolfcamp A, yielded the best results in both restricted fracture height growth and improved fracture half-length. This result was a function of the amount of depletion in the Lower Spraberry (i.e., lower stress) as well as the higher frequency of weak beds/interfaces in the Wolfcamp A.

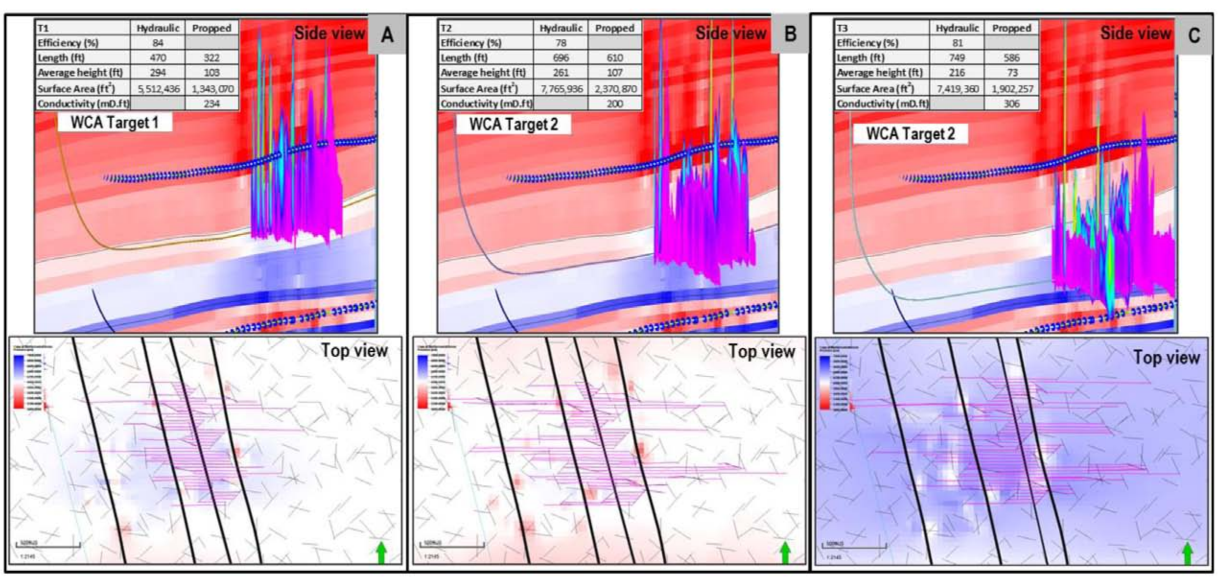

Figure 17—Hydraulic fracture geometry for all Wolfcamp A targets. (A) Target 1, Upper Wolfcamp A. (B) Target 2, Middle Wolfcamp A. (C) Target 3, Lower Wolfcamp A.

Forecasted production of these three scenarios (in conjunction with continued production from the parent wells) predicted that target 1 would result in the least production (Fig. 18). Targets 2 and 3 were predicted to yield 360% and 650% more oil production after 1 year, respectively. With the results clearly showing that deeper landing locations would result in more vertically confined fractures with longer half-lengths, the rest of the completion was then studied in detail.

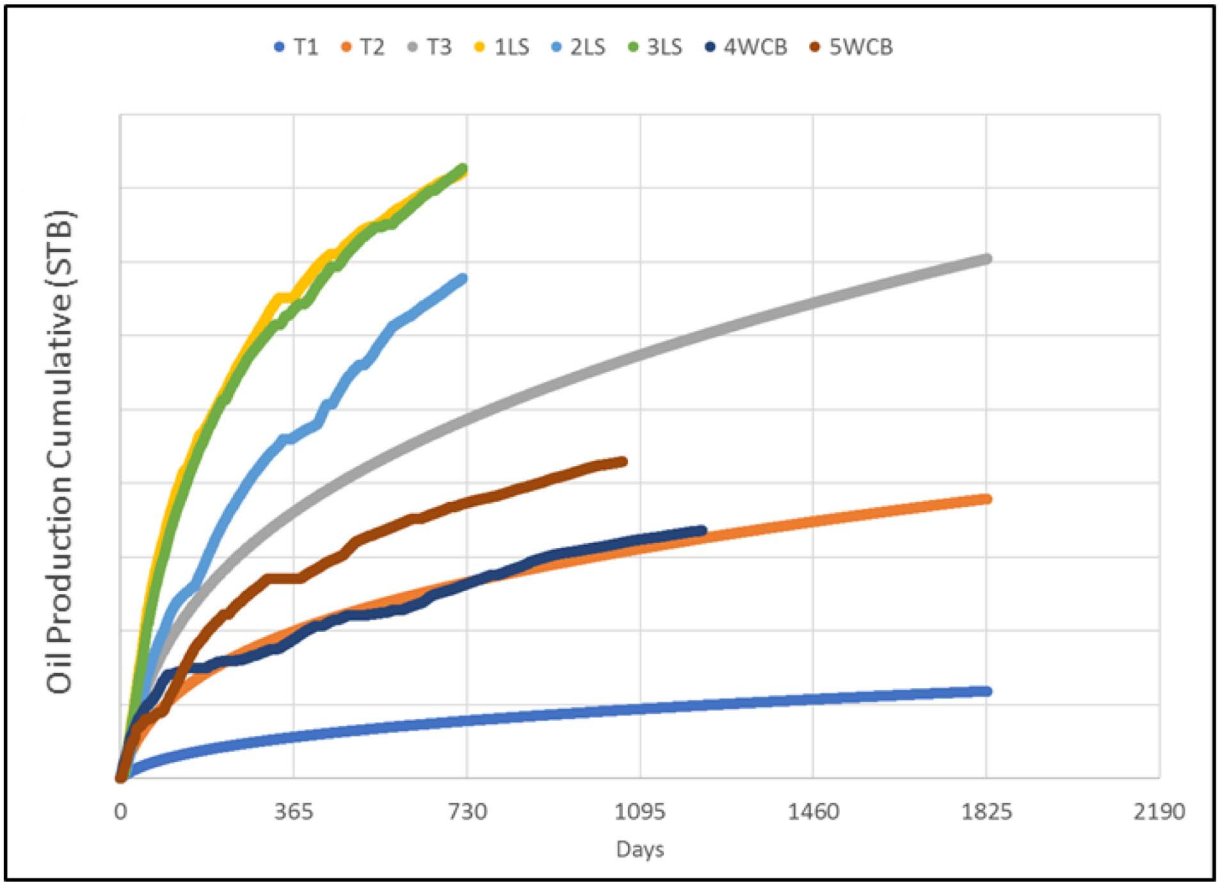

Figure 18—Cumulative oil production by well for the wells including Wolfcamp A targets.

Completion Optimization

Rather than persist with a completion design that was well suited to parent well completions, all aspects were explored to optimize the Wolfcamp A child well. The effects of all relevant parameters were simulated sequentially according to the matrix shown in Table 1, first focusing on one parameter (e.g., pumping rate), and then focusing on a variety of parameters in combination.

Table 1—Completion design sensitivities matrix

Sensitivities	Rate BPM	% Prop Type	Proppant Mass lbs/ft	Cluster Spacing ft	Stage Length ft
Base	**80**	**50% 100 mesh, 50% 40/70**	**1600**	**25**	**200**
Rate	*85*	50% 100 mesh, 50% 40/70	1600	25	200
	90	50% 100 mesh, 50% 40/70	1600	25	200
	100	50% 100 mesh, 50% 40/70	1600	25	200
% Proppant type	80	*100% 100 mesh, 0% 40/70*	1600	25	200
	80	*25% 100 mesh, 75% 40/70*	1600	25	200
	80	*50% 100 mesh, 50% 30/50*	1600	25	200
Proppant mass	80	50% 100 mesh, 50% 40/70	*1850*	25	200
	80	50% 100 mesh, 50% 40/70	*2000*	25	200
Clusters spacing	80	50% 100 mesh, 50% 40/70	1600	*14*	200
	80	50% 100 mesh, 50% 40/70	1600	*20*	200
Stage length	80	50% 100 mesh, 50% 40/70	1600	25	*125*
	80	50% 100 mesh, 50% 40/70	1600	25	*167*
	80	50% 100 mesh, 50% 40/70	1600	25	*250*
Additional test	85	50% 100 mesh, 50% 40/70	1850	14	200
	85	50% 100 mesh, 50% 40/70	1850	20	200
	80	50% 100 mesh, 50% 40/70	1850	14	200
	80	50% 100 mesh, 50% 40/70	1850	20	200

Fig. 19 shows the forecasted production of all five parent wells for each scenario in green, and the same five parent wells along with the child well production in blue (i.e., child well production being the differential between blue and green bars). Clearly superior parameter selections are highlighted in orange, and dashed lines indicating the totals for the base design are also included to assist comparison.

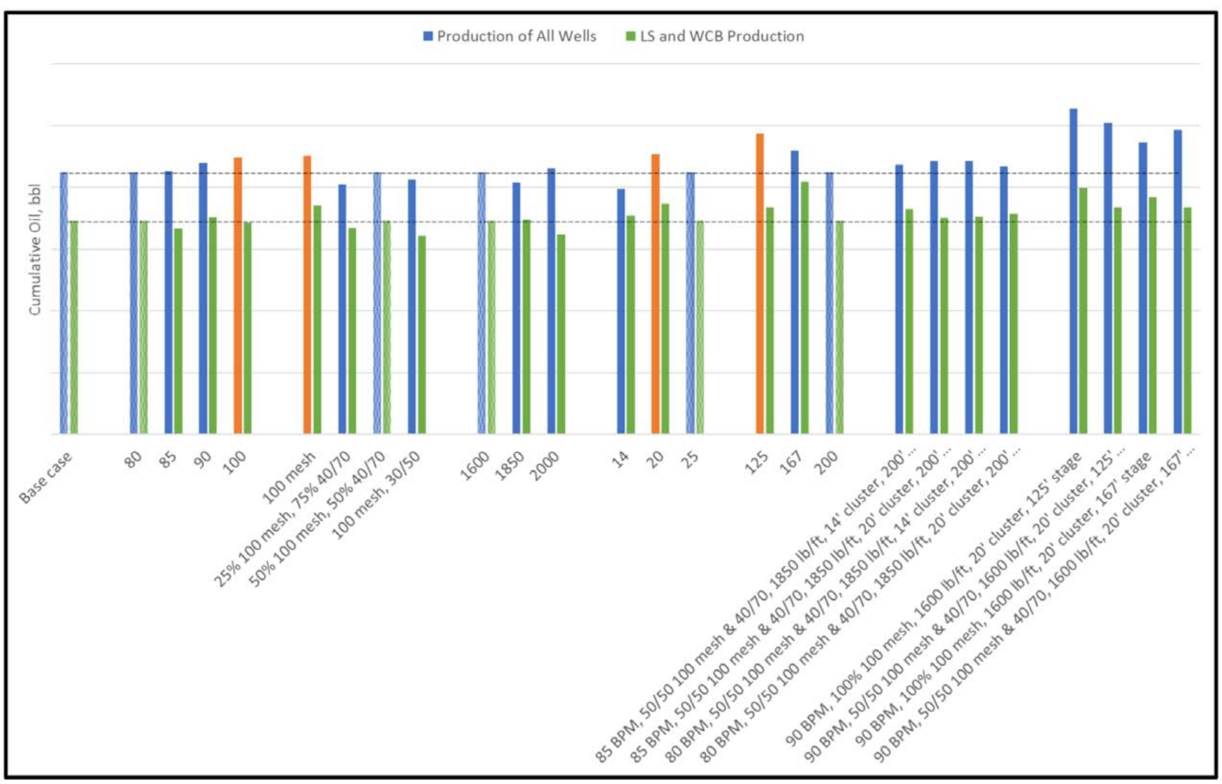

Figure 19—Forecasted production for each scenario in the completion design matrix in Table 1.

Increased pump rate appeared to be beneficial to cumulative oil production, although the benefits were unlikely to offset the costs associated with the increased horsepower. Designs integrating larger quantities of 100-mesh sand were predicted to be superior, likely due to the better transport properties of the proppant. Increased proppant masses were not expected to add to production performance. More fractures were predicted to be beneficial, but only to a point. The addition of more stages by way of reduced stage length was clearly beneficial, but a moderate cluster spacing of 20 ft was ideal. Tighter spacing was predicted to be hampered by stress shadow effects.

Following the identification of the completion parameters that could be optimized, combinations of the same were selected to identify the overall best design for the child well in the Wolfcamp A. Whereas a reduced stage length of 125 ft was identified as being ideal, the cost associated with this design was deemed to be too high and resulted in choosing a stage length of 167 ft (i.e., six stages per 1,000 ft). This was combined with a cluster spacing of 20 ft (i.e., eight clusters per stage) to keep the same number of perforation clusters per *stage* as the base design, while increasing the number of perforation clusters per *lateral foot* by 20%. Pumping rate was determined to be slightly beneficial, so the rate was increased to 90 bbl/min, but the proppant mass was not increased from the base design of 1,600 lbm/ft. Finally, a mixture of 50/50 100-mesh and 40/70-mesh sand was determined to be the ideal mix of proppant for the optimized design, mixing the advantages of the transport properties of 100-mesh sand with the added conductivity of the 40/70-mesh sand.

Conclusion

A comprehensive workflow for the optimization of a Wolfcamp A child well surrounded by five parent wells producing from the overlying Lower Spraberry and underlying Wolfcamp B has been introduced. This was accomplished by matching the stimulation pressures of each parent well to determine fracture geometry, matching the production from the same wells to determine pressure depletion, and then recalculating the in-situ stress field to reflect the changes in pore pressure. The updated stress field was reintegrated into a 3D model, with the results being used to simulate the effects of varying landing points and completion parameters of a child well to optimize production performance.

Initial results from the Wolfcamp A child wells adjacent to the modeled area with similar well configurations suggested that they were successfully optimized. Well 2WCA was landed and completed as recommended, and well 1WCA was landed shallower and completed as recommended. Early production performance of both child wells exceed most of the five parent wells within the same time period (Fig. 20).

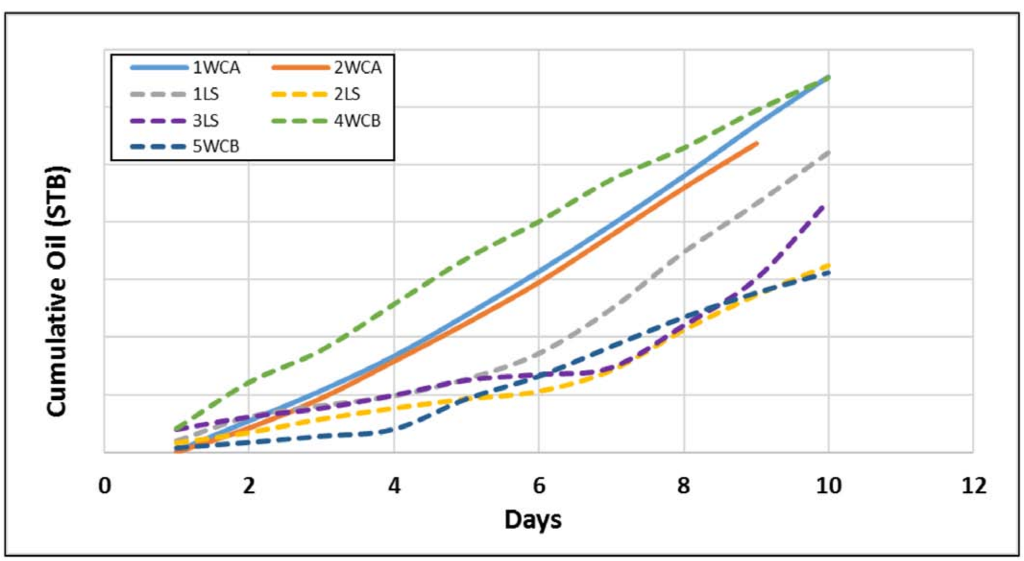

Figure 20—Actual flowback results from Wolfcamp A wells (solid lines) completed as recommended. The dotted lines represent production from parent wells within the same time period.

Acknowledgments

The authors would like to thank Diamondback Energy and Schlumberger for their permission to publish these results. Additionally, they would like to thank Russell Pantermuehl, Paul Molnar, Mike Hollis, Farhan Alimahomed, Helena Gamero Diaz, Efe Ejofodomi, Peter Kaufman, Garrett Lindsay, Eric Wigger and Bruce MacKay for their helpful discussions during the generation and execution of the workflow outlined in this paper.

References

Ajisafe, F., Solovyeva, I., Morales, A. et al. 2017. Impact of Well Spacing and Interference on Production Performance in Unconventional Reservoirs, Permian Basin. Presented at the Unconventional Resources Technology Conference, Austin, Texas, USA, 24–26 July. URTeC-2690466. https://doi.org/10.15530/urtec-2017-2690466.

Defeu, C., Garcia Ferrer, G., Ejofodomi, E. et al. 2018. Time Dependent Depletion of Parent Well and Impact on Well Spacing in the Wolfcamp Delaware Basin. Presented at SPE Liquids-Rich Basins Conference, Midland, Texas, USA, 5–6 September. SPE-191799-MS. https://doi.org/10.2118/191799-MS.

Diaz, H. G., Desroches, J., Williams, R. et al. 2018. Rock Fabric Analysis Based on Borehole Image Logs: Applications to Modeling Fracture Height Growth. Presented at SPE International Hydraulic Fracturing Technology Conference & Exhibition, Muscat, Oman, 16–18 October. SPE-191389-MS https://doi.org/10.2118/191389-18IHFT-MS

Ejofodomi, E. A., Baihly, J. D., and Silva, F. 2015. Using a Calibrated 3D Fracturing Simulator to Optimize Completions of Future Wells in the Eagle Ford Shale. Presented at the Unconventional Resources Technology Conference, San Antonio, Texas, USA, 20–22 July. URTEC-2172668-MS. https://doi.org/10.15530/URTEC-2015-2172668.

Gakhar, K., Shan, D., Rodionov, Y. et al. 2016. Engineered Approach for Multi-Well Pad Development in Eagle Ford Shale. Presented at the Unconventional Resources Technology Conference, San Antonio, Texas, USA, 1–3 August. URTeC-2431182. https://doi.org/10.15530/urtec-2016-2431182.

Gakhar, K., Rodionov, Y. Defeu, C. et al. 2017. Engineering an Effective Completion and Stimulation strategy for Infill Wells. Presented at the SPE Hydraulic Fracturing Technology Conference, The Woodlands, Texas, USA, 24–26 January. SPE-184835-MS. https://doi.org/10.2118/184835-MS.

Lindsay, G., Miller, T., Xu, T. et al. 2018. Production Performance of Infill Horizontal Wells vs. Pre-Existing Wells in the Major US Unconventional Basins. Presented at the SPE Hydraulic Fracturing Technology Conference, The Woodlands, Texas, USA, 23–25 January. SPE-189875-MS. https://doi.org/10.2118/189875-MS.

Malpani, R., Sinha, S., Charry, L. et al. 2015. Improving Hydrocarbon Recovery of Horizontal Shale Wells Through Refracturing. Presented at the SPE/CSUR Unconventional Resources Conference, Calgary, Alberta, Canada, 20–22 October. SPE-175920-MS. https://doi.org/10.2118/175920-MS.

Marongiu-Porcu, M., Lee, D., Shan, D. et al. 2015. Advanced Modeling of Interwell Fracturing Interference: An Eagle Ford Shale Oil Study. Presented at the SPE Annual Technical Conference and Exhibition, Houston, Texas, USA, 28–30 September. SPE-174902-MS. http://dx.doi.org/10.2118.174902-MS.

Martinez, R., Rosinski, J., and Dreher, D.T. 2012. Horizontal Pressure Sink Mitigation Completion Design: A Case Study in the Haynesville Shale. Presented at the SPE Annual Technical Conference and Exhibition, San Antonio, Texas, USA, 8–10 October: SPE-159089-MS. http://dx.doi.org/10.2118/159089-MS.

Wallace, K. J., Aguirre, P. R., Jinks, E. et al. 2016. Understanding Completion Performance in Niobrara-Codell Reservoirs Through the Use of Innovative Software-Guided Workflows and Models. Presented at SPE Hydraulic Fracturing Technology Conference, The Woodlands, Texas, USA, 9–11 February. SPE-179172-MS. https://doi.org/10.2118/179172-MS